Magnetic and structural studies of Sc containing ruthenate double perovskites A_2ScRuO_6 (A = Ba, Sr).

Paula Kayser, Sean Injac, Ben Ranjbar and Brendan J. Kennedy*

School of Chemistry, The University of Sydney, Sydney, NSW 2006, Australia

Maxim Avdeev

Australian Nuclear Science and Technology Organisation, Lucas Heights, NSW 2234, Australia

Kazunari Yamaura.

Research Center for Functional Material, National Institute for Materials Science, 1-1 Namiki, Tsukuba, Ibaraki 305-0044, Japan

Graduate School of Chemical Sciences and Engineering, Hokkaido University, North 10 West 8, Kita-ku, Sapporo, Hokkaido 060-0810, Japan

Brendan.Kennedy@sydney.edu.au

Abstract

Ruthenium containing double perovskites A_2ScRuO_6 have been synthesized as polycrystalline powders and structurally characterized using a combination of synchrotron X-ray and neutron powder diffraction methods. When *A* = Ba a hexagonal 6L perovskite structure is obtained if the synthesis is conducted at ambient pressure and a rock-salt ordered cubic structure obtained if the sample is quenched from high pressures. The Sr oxide Sr_2ScRuO_6 is obtained with a rock-salt ordered corner sharing topology. Heat capacity and bulk magnetic susceptibility measurements show the three oxides are antiferromagnets. Cubic Ba_2ScRuO_6 undergoes a metal-insulator transition near 270 K and hexagonal Ba_2ScRuO_6 is a semiconductor with an activation energy of 0.207 eV. The magnetic structures of the two rock-salt ordered double perovskites were established using powder neutron diffraction, and are described by $\boldsymbol{k}$ = (001) and $\boldsymbol{k}$ = (000) for the Ba and Sr oxides respectively, corresponding to type I antiferromagnetic structures, with ferromagnetic layers stacked antiferromagnetically. The ambient pressure hexagonal polymorph of Ba_2ScRuO_6 has partial Sc-Ru ordering at both the face-sharing B_2O_9 dimer and corner sharing BO_6 sites. The magnetic structure is described by $\boldsymbol{k}$ = (½ 0 0) with the basis vector belonging to the irreducible representation Γ^3.

Introduction

The ruthenate perovskites have attracted attention ever since the discovery of ferromagnetism in $SrRuO_3$ [1] and considerable efforts have been directed at understanding, and enhancing the ferromagnetism by chemical doping [2-4]. Considering the general perovskite as ABO_3, if the *B*-site contains two cations in a 1:1 ratio, ordering of these can occur provided there are sufficient differences in their size and/or charge [5, 6]. Such ordered systems are generally referred to as double perovskites and for the ruthenates they have the general formula A_2BRuO_6 where *A* is a large cation such as Ba^{2+}, Sr^{2+} or La^{3+} and the *B*-cation a smaller metal [7-19]. The oxidation state of the Ru is related to the valence of the other cations with the much of interest focused on systems containing Ru^{5+} (t_{2g}^3, S=3/2) cations.

If the *B*-site in a ruthenate with an ordered double perovskite structure is non-magnetic, such as Y^{3+}, there is the potential for magnetic frustration [15, 19]. Since the Ru and *B*-type cations are placed at non-equivalent crystallographic sites, each sublattice forms a face-centered cubic arrangement, which is equivalent to a network of edge-sharing tetrahedra, and therefore, the antiferromagnetic nearest-neighbour interactions are frustrated. A number of Ru^{5+} double perovskites show long range antiferromagnetic ordering including Sr_2YRuO_6 and Ba_2YRuO_6 despite the high levels of frustration [13, 15, 17].

The magnetism in double perovskites, especially those containing cations with a half-filled t_{2g}^3, S=3/2 configuration (Ru^{5+}, Os^{5+}, and Ir^{6+}) has been the subject of recent debate and interest [10, 20, 21]. It is emerging that spin-orbit coupling (SOC) plays a significant role influencing the magnetic properties of the 5*d* containing oxides and it is increasingly believed that this is also significant in 4*d* oxides [22]. Thompson and co-workers [23] recently demonstrated a correlation between the ordered magnetic moments in nd^3 perovskites and the spin-orbit coupling constant. Studies of Sr_2ScOsO_6 indicate that SOC-induced anisotropy combined with strong nearest-neighbour magnetic interactions stabilise high magnetic ordering temperature, 92 K [24-26]. That this is considerably higher than the ordering temperature in Sr_2YOsO_6, 53 K despite their very similar structures, suggests the non-magnetic *B*-cation plays a significant role in influencing the strength of the magnetic interactions. Calculations of the Sr_2BOsO_6 (B = Y, In, Sc) oxides support this suggestion [26, 27].

Surprisingly very little is known about the mixed Ru-Sc double perovskites. The interesting results for the ruthenates and osmates described above encouraged us to study the analogous Ba_2ScRuO_6 and Sr_2ScRuO_6 double perovskite. We have identified that Ba_2ScRuO_6 can be prepared with two structural forms, a hexagonal form if prepared at ambient pressure (AP- Ba_2ScRuO_6) and a cubic form if prepared at high pressure (HP- Ba_2ScRuO_6). The magnetic properties and crystal and magnetic structures of these oxides are described.

Experimental

Polycrystalline samples of AP-Ba_2ScRuO_6 and Sr_2ScRuO_6 were prepared by solid state reaction. An appropriate stoichiometric mixture of $BaCO_3$ (Aldrich, 99.999 %), $SrCO_3$ (Aldrich, 99.99 %), Sc_2O_3 (Aldrich, 99.999 %) and Ru powder (Aithaca, 99.9 %) was weighed and finely mixed by hand in an agate mortar. Prior to weighing the $BaCO_3$ and $SrCO_3$ were dried at 150 °C for 12 hours and Sc_2O_3 was heated at 1000 °C for 12 hours. The samples were placed in alumina crucibles and heated at 650 °C for 12 hours and 850 °C for 12 hours with intermediate regrinding. After mixing again, the samples were pressed into 20 mm diameter pellets and heated in air at 1050 °C for 24 hours, 1200 °C for 72 hours and 1400 °C for 72 hours. The Ba_2ScRuO_6 sample was finally heated at 1450 °C for 72 hours. The samples were cooled to ambient temperature in the furnace at a rate of 5°C/min.

HP-Ba_2ScRuO_6 was prepared from fine powders of BaO_2 (Kojundo Chemical Laboratory, 99%), Sc_2O_3 (Kojundo Chemical Laboratory, 99.9%), RuO_2 (Rare Metallic, 99.9%), and Ru (Strem Chemicals, 99.99%). It is not feasible to use carbonates in the synthesis due to the release of CO_2. These powders were mixed at stoichiometric and oxygen-over-stoichiometric (3 and 6 at% excesses) ratios in an argon glovebox, followed by sealing the mixtures – each ~0.4 g– in Pt capsules. The capsule was compressed isotropically in a multi-anvil-type apparatus to elevate the applied pressure to be at 6 GPa. Subsequently, it was heated at 1500 °C for 30 min with maintaining the pressure. After the capsule was quenched to room temperature within a minute, it was gradually depressurized over 3 hrs.

Synchrotron X-ray powder diffraction data were collected over the angular range $5 < 2\theta < 85°$, using X-rays of wavelength 0.82465 or 0.58993 Å, as determined by structural refinement of a diluted NIST SRM660b LaB_6 standard, on the powder diffractometer at BL-10 beamline of the Australian Synchrotron [28]. The samples were housed in 0.2 mm diameter capillaries that were rotated during the measurements. For the neutron diffraction measurements the sample was sealed in a 6 mm diameter vanadium can and the neutron powder diffraction data were obtained using the high resolution powder diffractometer Echidna at ANSTO's OPAL facility at Lucas Heights [29]. The wavelengths of the incident neutrons, obtained using (335) and (331) reflections of a germanium monochromator, were 1.6220 Å and 2.4395 Å, respectively, as determined using data collected for a certified NIST SRM660b LaB_6 standard. This instrument has a maximum resolution of $\Delta d/d \sim 1 \times 10^{-3}$. Structure refinements using the Rietveld method were carried out using the GSAS [30] program with the EXPGUI [31] front-end (non-magnetic structures) or Fullprof [32] (magnetically ordered structures). Since the magnetic form factor of Ru^{5+} is not listed in *The International Tables of Crystallography* Parkinson *et al.*[33] estimated this using a common scaling factor of the exponent in each exponential term of the next element or ionic state. The Ru^{5+} magnetic form factor used in this work was A ~

0.441, a ~ 21.046 (33.309), B ~ 1.4775, b ~ 6.0360 (9.553), C ~ 20.9361, c ~ 4.2473 (6.722) and D ~ 0.0176, obtained using the magnetic form factor of Ru^{+} (value shown in parenthesis) and a scale factor of 0.63184. This allowed accurate magnetic moment of the Ru^{5+} cations to be refined.

DC magnetic susceptibilities were measured using a Quantum Design PPMS9. Zero- field cooled (ZFC) and field-cooled (FC) magnetic susceptibility data were measured with a magnetic field of 1000 Oe and the isothermal magnetization curves were obtained for magnetic fields from -3 T to 3 T at 4 and 100 K using the vibrating sample magnetometer technique. Heat capacity and resistivity measurements were collected on the same platform using a thermal relaxation and four-probe DC methods respectively.

Results and Discussion

(i) Physical Property Measurements

The molar magnetic susceptibilities of Sr_2ScRuO_6 show a maximum near 33 K and a pronounced feature near 64 K indicating antiferromagnetic ordering, see Figure 1. The heat capacity shows that the Neel temperature corresponds to the higher of these temperatures, with a lambda type feature seen in the specific heat measurements at T_N = 60 K. A second feature is obvious in the heat capacity measurements, at 126 K, that has no corresponding feature in the susceptibility plot, demonstrating this is structural in origin. This was confirmed in the structural studies described below. Attempts to measure the conductivity of the sample were unsuccessful as a result of the high resistivity of the sample.

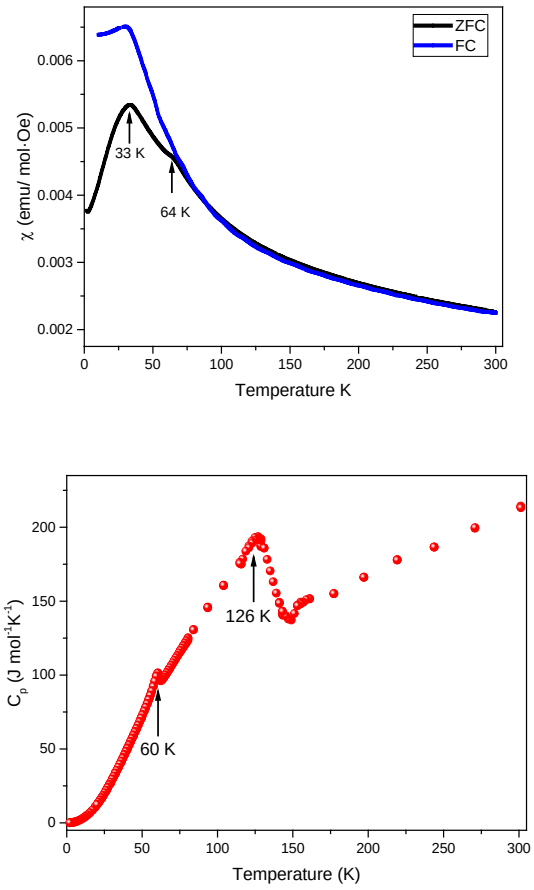

Figure 1. Temperature dependence of the dc magnetic susceptibility measured under a 1000 Oe magnetic field, and the heat capacity for Sr_2ScRuO_6.

Bulk magnetic susceptibility measurements of HP-Ba_2ScRuO_6 demonstrate that this undergoes antiferromagnetic ordering near 44 K, Figure 2. There is a slight divergence of the field-cooled (FC) and zero field-cooled (ZFC) susceptibility plots at temperatures above this. The temperature dependence of the ZFC susceptibilities suggest there are two ordering temperatures T_N = 44 K and 31 K, although heat capacity measurements suggest that true long range ordering occurs at the higher of the two temperatures. Due to the small sample volume available from the high pressure synthesis it was not feasible to investigate the possibility of diffuse magnetic scattering persisting to above T_N as observed in Ba_2YRuO_6 and Sr_2YRuO_6 [15, 17, 19]. The heat capacity measurements also revealed a small anomaly near 145 K, that has no corresponding feature in the magnetic susceptibly behavior, nor in the structural studies described below. Since non-magnetic analogues of tall three phases studied here are not available we have not attempted to the magnetic contribution to the heat capacity by subtraction of the lattice contribution. Finally resistivity measurements showed a sharp increase in resistivity as the sample is cooled below 270 K, indicative of a metal-insulator transition. Similar results were obtained for duplicate samples.

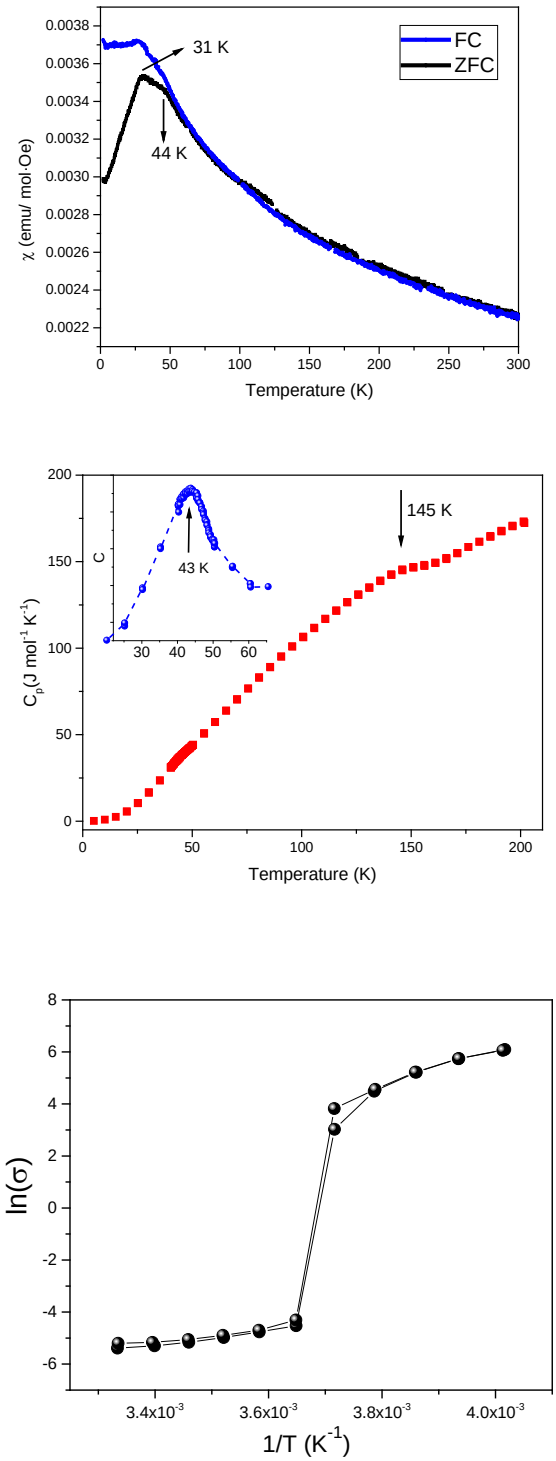

Figure 2. Temperature dependence of the dc magnetic susceptibility measured under a 1000 Oe magnetic field, heat capacity and resistance for HP- Ba_2ScRuO_6. The inset in the heat capacity plot shows the magnetic contribution, were the lattice and electronic contributions, modelled using a polynomial function, were subtracted.

Finally magnetic susceptibility measurements of AP-Ba_2ScRuO_6 showed a single AFM peak near 8K. In this case the FC and ZFC susceptibilities are essentially identical at temperature above this, Figure 3. The temperature dependence of the resistivity of AP-Ba_2ScRuO_6 is typical of a semi-conductor, with a small anomaly apparent near 260 K, Figure 3. This temperature is similar to that observed for the metal-insulator transition in the cubic polymorph and it is likely that this is due to the presence of a small amount of the cubic phase evident in the SXRD data, described below. The activation energy was estimated to be 0.207 eV at temperatures below this and 0.202 eV above this. Application of a 1T magnetic field shifted the temperature of the anomaly slightly and resulted in a small decrease in the activation energy to 0.191 eV. The heat capacity shows a weak feature near 35 K (most obvious in the Cp/T vs T plot) that is believed to be associated with the magnetic ordering, although it may reflect the presence of a small amount of the cubic phase in the sample, as well as a feature near room temperature, that we show below is associated with a structural transition.

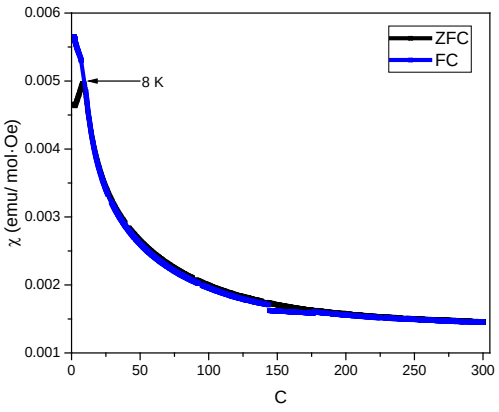

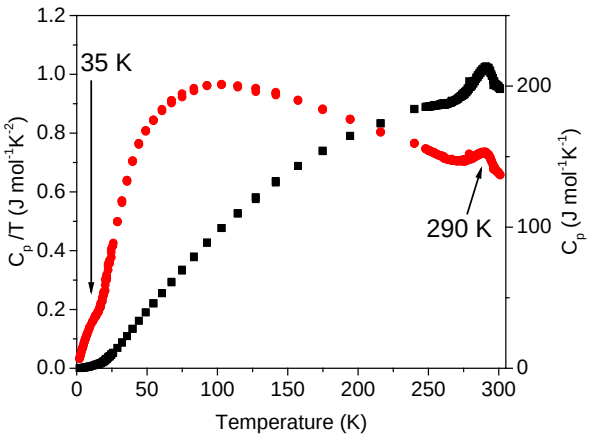

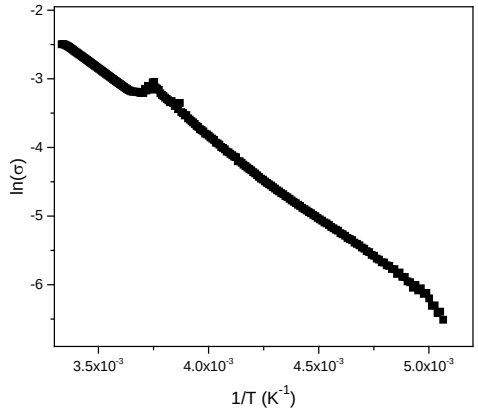

Figure 3. Temperature dependence of the dc magnetic susceptibility measured under a 1000 Oe magnetic field, heat capacity and resistance for AP- Ba_2ScRuO_6.

(ii) Room Temperature Structures

A combination of NPD and S-XRD was employed to first identify the appropriate symmetry of both forms of Ba_2ScRuO_6 and of Sr_2ScRuO_6 and then to refine their structures. Examination of the peak splitting in the S-XRD pattern showed Sr_2ScRuO_6 to be monoclinic with space group either $P2_1/n$ or $I2/m$. Examination of the observed intensities of the superlattice peaks in the NPD profile demonstrated that space group $I2/m$ was appropriate, and the structure was refined in this space group. $I2/m$ differs from the more commonly observed $P2_1/n$ space group by the absence of in-phase tilts and is described by the Glazer notation ($a^-a^-c^0$) [34]. Trace amounts of Sc_2O_3 were observed in the diffraction data and this was considered as a second phase in the refinements. The refined bond distances are given in Table 1 and these, together with the derived BVS of 4.93 are indicative of Ru^V. The Sc-O distances are somewhat shorter than expected, the average Sc-O distance is 2.02 Å and the derived BVS is 3.33. A similar anomaly is observed in the analogous Ir and Os oxides Sr_2ScIrO_6 and Sr_2ScOsO_6, where the Sc bond valences are 3.65 and 3.45 respectively [35] [25]. The difference in the number of electrons, as well as in the neutron scattering length between the Sc (12.29 fm) and Ru (7.03 fm) atoms, provided considerable sensitivity to Sc-Ru ordering over the two *B*-sites and the structural refinements provided no evidence for any anti-site disorder.

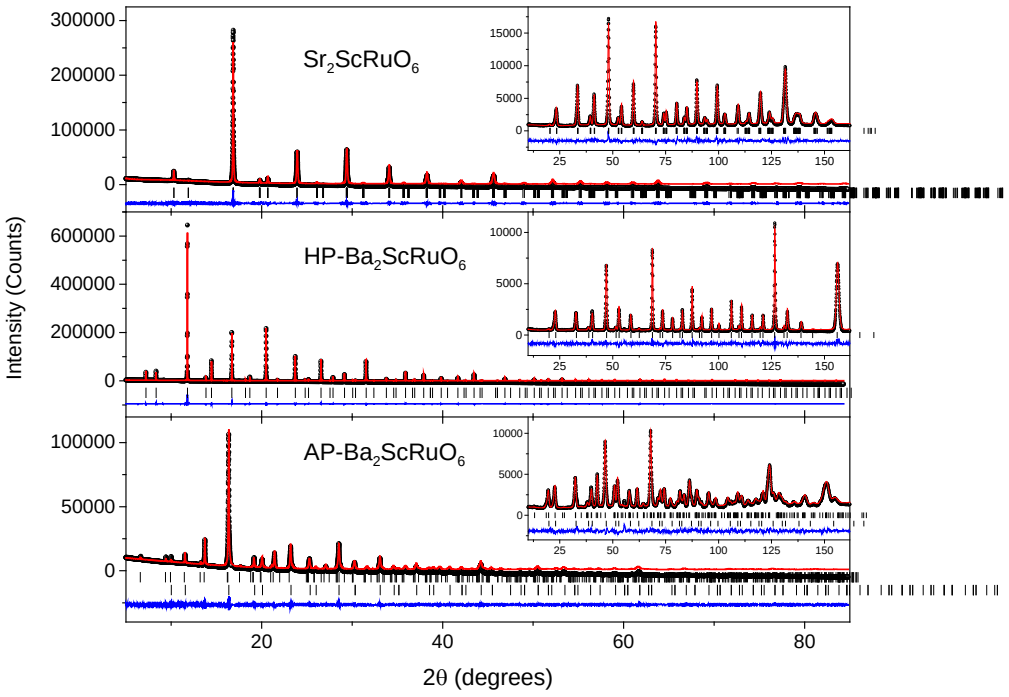

Figure 4. Rietveld refinement profiles for S-XRD and NPD (inset) patterns of Sr_2ScRuO_6 and the two samples of Ba_2ScRuO_6 at room temperature. The symbols are the experimental data and the solid line the fit to the profile. In each case the difference between the observed and calculated profiles is given in the lower solid line, and the vertical markers show the positions of the space group allowed Bragg reflections. The lower set of vertical markers in the profiles of AP-Ba_2ScRuO_6 is due to the presence of a small amount of a cubic phase. For clarity the reflection markers due to trace amounts of Sc_2O_3 have not been included, these are illustrated in Figure 9 and 11.The S-XRD data for Sr_2ScRuO_6 and AP-Ba_2ScRuO_6 were collected at $\lambda = 0.82465$ Å and for HP- Ba_2ScRuO_6 at 0.58993 Å.

Table 1. Refined structural parameters for Sr_2ScRuO_6 at room temperature. The structure was refined in the monoclinic space group *I*2/*m* using a combined S-XRD and ND data set.

Atom	x	y	z	Ui/Ue*100/Å^2
Sr	0.4967(11)	0	0.2395(8)	1.71(4)
Sc	0	0	½	2.61(7)
Ru	0	0	0	0.72(6)
O1	-0.0424(9)	0	0.2461(8)	2.57(8)
O2	0.2346(16)	0.2427(18)	0.0129(8)	3.27(36)
Sc-O1 (x 2)	2.039(7)		Ru-O1(x 2)	1.976(7)

Sc-O2 (x 4)	2.008(3)		Ru-O2(x 4)	1.901(3)
BVS	3.33			4.93
	Sc-O1-Ru	166.3(3)°		
	Sc-O2-Ru	173.8 (4)°		

a = 5.6204(3) b = 5.6268(3) c = 7.9792(4) Å β = 89.770(4)° V= 252.34(2) Å^3
Neutron R_p=3.78 % R_{wp}=4.76 % S-XRD R_p=3.76 % R_{wp} = 5.40 % χ^2 =12.33

The S-XRD diffraction pattern of the sample of Ba_2ScRuO_6 prepared at 6 GPa, demonstrates this to be cubic, and the data was analysed using space group ($Fm\bar{3}m$). The lattice parameter was refined to be 8.12119(4) Å using a combined NPD-S-XRD data set, further details are given in Table 2. The refined Ru-O and Sc-O bond distances were 1.9850(9) and 2.0755(9) respectively. The slightly longer than expected Ru-O bond length is believed to be a consequence of the presence of a small amount of Ru-Sc antisite disorder, estimated to be 7.3(1) %, although the derived BVS appear reasonable.

Table 2. Refined structural parameters for HP-Ba_2ScRuO_6 at room temperature. The structure was refined in the cubic space group $Fm\bar{3}m$ using a combined S-XRD and ND data set.

Atom	*x*	*y*	*z*	Ui/Ue*100/Å^2	n
Sr	¼	¼	¼	0.504(2)	1
Sc	0	0	0	-0.09(9)	0.927(1)
Ru	½	0	0	0.70(1)	0.073(1)
O	0.25557(11)	0	0	0.53(8)	1
Sc-O (x 6)	2.0755(9)		Ru-O (x 6)	1.9850(9)	
BVS	3.25			4.77	

a = 8.12119(4) Å V= 535.622(7) Å^3
Neutron R_p=4.85 % R_{wp}=6.23 % S-XRD R_p=4.40 % R_{wp} = 6.10 % χ^2 =4.46

The S-XRD profile for the sample of Ba_2ScRuO_6 prepared at ambient pressure indicated that this adopted a 6L-type hexagonal perovskite-type structure in space group $P\bar{3}m1$ with a = 5.79649 (4) c = 14.2594(2) Å as originally described by Bader and Kemmler [36]. The structure consists of face sharing M_2O_9 dimeric units connected by single corner sharing MO_6 units and involves Sc and Ru ordering in alternate (001) layers as shown in Figure 5. Close examination of the diffraction patterns for Ba_2ScRuO_6 indicated that, although the major phase was hexagonal, a small amount of a cubic phase ($Fm\bar{3}m$ a = 8.1359 (Å)) was also present and this was included in the structural refinements. Since there is no obvious pathway between these two structures any transition between them must be first order and hence allows for the possibility of phase co-existence. Disorder of the Ru and Sc

cations was considered during the structural refinements and this indicated that Sc(1) and Ru(2) sites were exclusively occupied by the appropriate cation, but that the Sc and Ru were disordered over the other two sites. The Ru(3)/Sc(3) site was predominantly occupied by Sc 88.9(1.1)% and the Ru(4)/Sc(4) site by Ru 67.7(1.0)%. This corresponds to a refined stoichiometry of $Ba_2Ru_{1.15}Sc_{0.85}O_6$, although for simplicity this is described hereafter by the nominal stoichiometry of Ba_2ScRuO_6. There is evidence for a small amount of Sc_2O_3 in the samples. Refinements of the site occupancy factors of the oxygen atoms did not reveal significant changes from full occupancy and therefore these were fixed.

The tendency for the Ru to favour the face sharing positions is reminiscent of the behaviour in the 6H type perovskites $Ba_3Ru_2LnO_9$ [37-39]. Feng *et al.* [40] have recently reported that Ba_2FeOsO_6 adopts the same 6L-type structure as observed here. The degree of Fe/Os disorder in Ba_2FeOsO_6 is much greater than that seen for AP-Ba_2ScRuO_6. Selected bond lengths are listed in Table 3. The $Sc(1)O_6$ and $Sc(3)O_6$ polyhedra are constrained by symmetry to have six equal bonds whereas the *M*(2) and *M*(4) octahedra are less regular with three shorter *M*-O distances and three longer ones. The metal-metal (*M-M*) distance across the shared face is 2.613(3) Å is less than the shortest contact in ruthenium metal (2.65 Å) suggestive of a strong attractive interaction. The distance across the shared face in Ba_2TeCoO_6, which also adopts a 6L-type hexagonal perovskite-type structure, is shorter again at 2.572(2) Å [41]. The distance observed for AP-Ba_2ScRuO_6 is similar to that found in $BaRuO_3$ [42]. Santoro *et al.* [43] have suggested that *M-M* repulsion across the faces can be minimised by contraction of the face, which is reflected by the relatively short non-bonding O1-O1 distance of 2.670(3) Å. The corresponding distance in the 9R polymorph of $BaRuO_3$ is 2.698(3) Å [42]. However, whereas in 9R-$BaRuO_3$ the distance across the corner sharing units is noticeably longer than that across the face sharing units, in Ba_2ScRuO_6 the O2-O2 distance is comparably short 2.673(3) Å, although the O3-O3 distance is considerably longer at 2.929 (5) Å. Similar patterns are seen in Ba_2TeCoO_6 where the O3-O3 distance of 2.982(4) Å is considerably longer than the O1-O1 and O2-O2 distances of 2.661(4) and 2.729(7) Å respectively. The Ru2-O1 distance is considerably longer than the Ru2-O2 distance 2.130(9) vs 1.869(10) Å. The Ru4 octahedron shows a similar, although not as large, bond distance anisotropy. Similar distortions were noted by Feng *et al.* [40] in Ba_2FeOsO_6, as well as at the dimer positions of other hexagonal perovkites such as $Ba_3NaOs_2O_9$ or $K_3NaOs_2O_9$ and it has been suggested that this is related with the displacement of the metal out of the centre of the octahedral [44 45]. A similar effect is observed here and in Ba_2TeCoO_6 [41] argues and it is tempting to suggest that the disorder of the cations somehow impacts on the attractive interactions of the cations across the shared face. The BVS of the Ru and Sc sites are unusual but consistent with the *M*3 site being Sc rich and the *M*4 site being Ru rich. More examples would be required to understand the significance of the octahedral distortion.

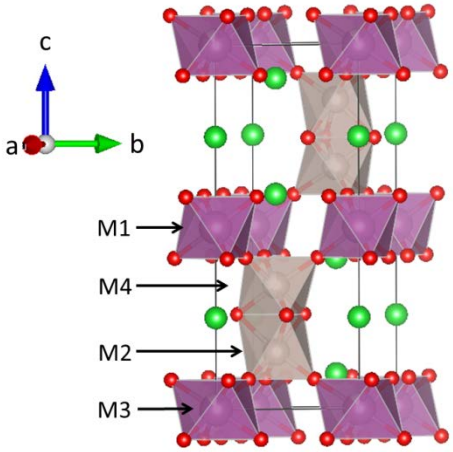

Figure 5. Representation of the 6L perovskite structure of Ba_2ScRuO_6. The Ba and O atoms are represented by green and red spheres respectively and the Sc and Ru cations occupy the centre of the polyhedra, with the Ru preferentially occupying the face sharing M2 and M4 sites and the Sc the corner sharing M1 and M3 sites.

Table 3. Refined structural parameters for the ambient pressure phase of Ba_2ScRuO_6. The structure was refined in the hexagonal space group $P\bar{3}m1$ using a combined S-XRD and NPD data set.

Atom	Site	*x*	*y*	*z*	Ui/Ue*100/Å^2	n
Ba1	2*c*	0	0	0.2518(5)	0.79(4)	1
Ba2	2*d*	1/3	2/3	0.0931(4)	0.41(10)	1
Ba3	2*d*	1/3	2/3	0.4113(4)	1.70(13)	1
Sc1	1*b*	0	0	½	0.51(32)	1
Ru2	2*d*	1/3	2/3	0.8448(4)	0.14(11)	1
Sc3	1*a*	0	0	0	0.42(30)	0.889(11)
Ru3	1*a*	0	0	0	0.42(30)	0.111(11)
Sc4	2*d*	1/3	2/3	0.6616(6)	0.89(17)	0.323(10)
Ru4	2*d*	1/3	2/3	0.6616(6)	0.89(17)	0.677(10)
O1	6*i*	0.5131(4)	-0.5131(4)	0.2583(7)	0.36(14)	1
O2	6*i*	0.8204(9)	-0.8204(9)	0.0813(6)	1.09(23)	1
O3	6*i*	0.8351(9)	-0.8351(9)	0.4153(5)	-0.27(19)	1
			Bond Length Å		BVS	
Sc1 – O3 (x 6)			2.049(9)		3.50	

Ru2 – O1 (x 3)	2.130(9)	4.27
Ru2 – O2 (x 3)	1.869(10)	
Ru3/Sc3 – O2 (x 6)	2.144(9)	2.70
Ru4/Sc4 – O1 (x 3)	1.919(8)	4.43
Ru4-Sc4 – O3 (x 3)	2.015(10)	

a = 5.79649 (4) c = 14.2594(2) Å V= *414.919(5)*Å^3
Neutron R_p 4.99 % R_{wp} 6.50 % S-XRD R_p 3.86 % R_{wp} 5.58 % χ^2 8.67

(iii) Low temperature Structures

Cooling Sr_2ScRuO_6 to 100 K resulted in the appearance of additional very weak reflections in the NPD profiles that were indexed as the 012 at d = 3.24 Å and the 210/120 near d = 2.52 Å. These peaks are associated with softening at the *M*-point due to the formation of in-phase tilts. This demonstrates that a transition to space group $P2_1/n$ (Glazer tilt system $a^-a^-c^+$) had occurred [34]. Cooling to 50 K resulted in the appearance of additional low-angle reflections associated with the magnetic contribution to the scattering indicative of long-range antiferromagnetic ordering, see Figure 6. These changes are reflected in the heat capacity measurements that reveal two transitions, the first near 126 K that is due to the $I2/m - P2_1/n$ structural transition and the second near 60 K that is due to the onset of long range antiferromagnetic ordering (Figure 1).

The magnetic propagation vector was calculated by using K_SEARCH and the subsequent determination of the magnetic structure was accompanied using BasIreps as implemented in Fullprof. All of the magnetic peaks in the low temperature NPD pattern were indexed with the propagation vector $\boldsymbol{k}$ = (000), thus the magnetic unit cell coincides with the chemical one. From the analysis of the possible magnetic structures compatible with this propagation vector and the space-group $P2_1/n$, the best agreement with the experimental data was obtained for the spin arrangement where the Ru1(0,0,0) and Ru2 (½,½,½) spins are magnetically coupled as $m_{1x} = -m_{2x}$, $m_{1z} = -m_{2z}$, corresponding to the Irep Γ^1. The refined components of the magnetic moment at 3 K, along the crystallographic *a*- and *c*-axes, are m_x = 1.80(6) μ_B and m_z = 0.8(1) μB, and the net moment is 1.97(2) μ_B. As shown in Figure 7, the magnetic structure consists of ferromagnetic (001) layers of Ru^{5+} moments coupled antiferromagnetically along [001], characteristic of a type-I AFM structure. This is the same magnetic structure seen in Sr_2YRuO_6 [12, 17, 46]. The frustration index, $f = |\theta_c|/T_N$ where θ_c is the Curie temperature determined from bulk susceptibility measurements and T_N the Neel temperature is 4 indicating substantial frustration in the system. The value of the magnetic moment estimated from the Curie-Weiss fitting of the susceptibility data between 150 and 300 K is 3.1 μB and θ_c = -242 K.

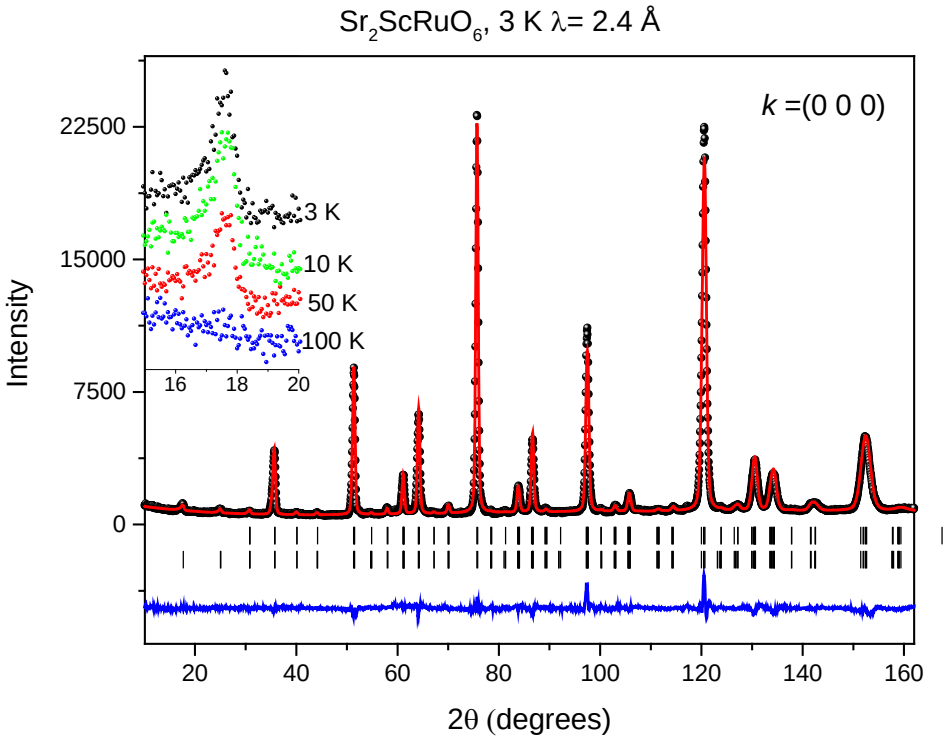

Figure 6. Observed (symbols), calculated (red line), and difference (blue line) NPD Rietveld profiles for Sr_2ScRuO_6 at 3 K. The first series of Bragg reflections corresponds to the main perovskite phase and the second one to the magnetic structure. The inset shows the appearance of the magnetic (001) reflection at low temperatures.

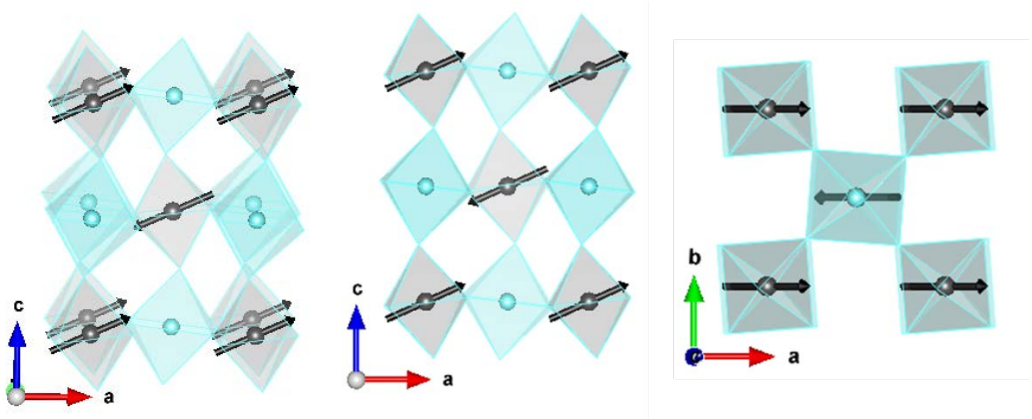

Figure 7. Schematic view of the magnetic structure of Sr_2ScRuO_6 below T_N.

A NPD pattern was measured for HP-Ba_2ScRuO_6 at 3K and this showed that the structure remained cubic, suggesting the feature at 145 K seen in the heat capacity measurements is not a consequence of a structural transition associated with the introduction of cooperative tilting of the

corner sharing octahedra. Consequently S-XRD data were collected for HP-Ba_2ScRuO_6 at relatively fine temperature intervals between 85 and 300 K to further search for a structural basis of this feature. These data showed no indication of any change in symmetry upon cooling and in particular the patterns measured at 125 and 175 K, immediately above and below the anomaly observed in the heat capacity measurements were essentially identical. The thermal expansion of the cubic lattice parameter between 85 and 300 K is unexceptional and is fitted by a quadratic $a = 8.10856 + 1.7026 \times 10^{-5}T + 1.0337 \times 10^{-7}T^2$, see Figure 8. The magnetic structure of the cubic polymorph of Ba_2ScRuO_6 at 3 K was determined using neutrons of wavelength 2.4 and 1.6 Å, the latter increasing the precision of the refinements. The low-angle reflections at 2θ ~ 17 and 24° (*d* ~ 8.1 and 5.7 Å), evident in Figure 9 that are associated with the magnetic contribution to the scattering, were indexed with the propagation vector $\boldsymbol{k}$ = (001), as described above. In this system, the long-range magnetic order is exclusively due to Ru^{5+} ions which form a face-centered-cubic (fcc) sublattice, equivalent to an edge-sharing tetrahedral framework. From the analysis of the possible magnetic structures compatible with this propagation vector and the space-group $Fm\bar{3}m$, the best agreement with the experimental data was obtained for the spin arrangement where the Ru (0,0,0) moments are orientated along one of the cubic axis; the *a*-axis has been chosen arbitrary since the actual moment direction cannot be determined from a powder experiment in the cubic symmetry. The magnetic structure can be described as ferromagnetic *ab*-planes of Ru^{5+} moments coupled antiferromagnetically along *c*-axis, characteristic of a type-I anti-ferromagnetic structure (AFM) structure, as shown in Figure 10. The refined net magnetic moment is m_{mag} = 2.04(5) μ_B. The magnetic structure is similar to that described for Ba_2YRuO_6 [15, 19]. The value of the magnetic moment estimated from the Curie-Weiss fitting of the susceptibility data is 4.1 μB and θ_c = -651 K. which gives a frustration index of 15.

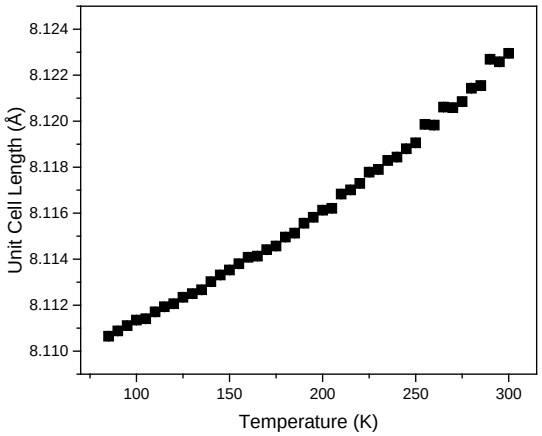

Figure 8. Thermal evolution of the unit-cell parameter of HP-Ba_2ScRuO_6 perovskite collected at powder diffractometer at BL-10 beamline of the Australian Synchrotron.

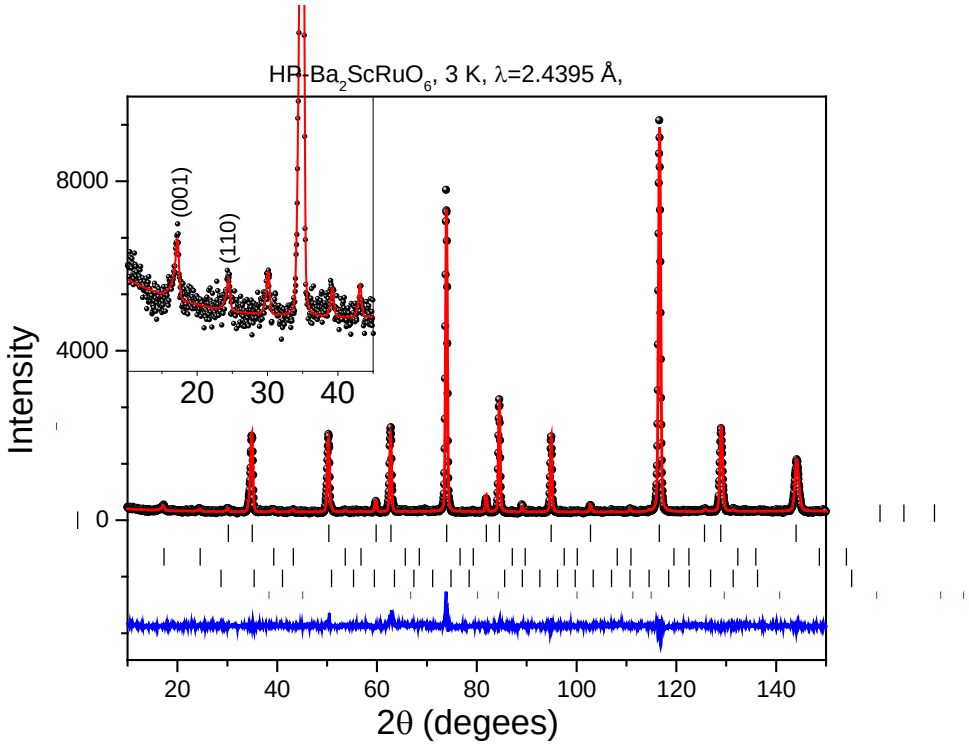

Figure 9. Observed (symbols), calculated (red line), and difference (blue line) NPD Rietveld profiles for HP-Ba_2ScRuO_6 at 3 K. The first series of Bragg reflections corresponds to the main perovskite phase and the second one to the magnetic structure. The lower set is from a Sc_2O_3 impurity. The inset highlights the appearance of the magnetic (001) and (110) reflection at low temperatures.

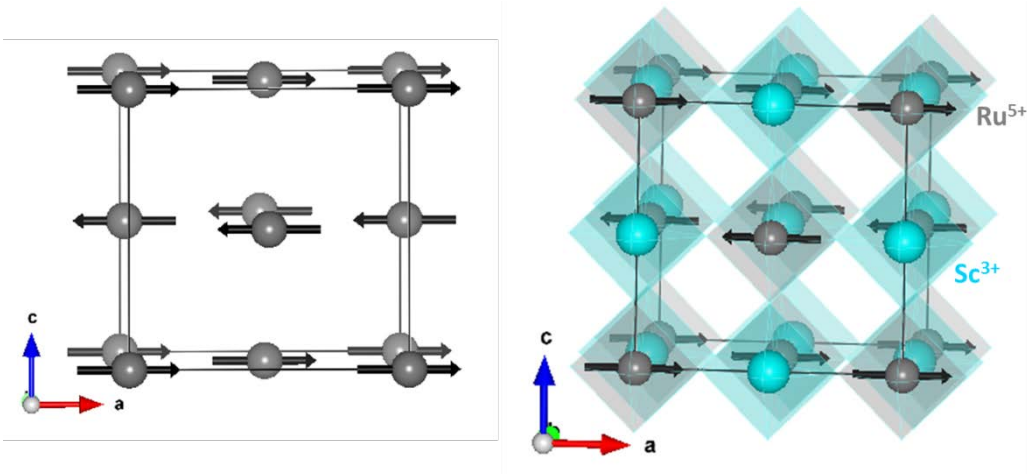

Figure 10. Schematic view of the magnetic structure of HP-Ba_2ScRuO_6 below T_N.

In the Rietveld refinement against NPD data for AP-Ba_2ScRuO_6 at 3K it was assumed that the Sc-Ru antisite disorder was the same as that determined at RT. The refined NPD profiles for this are shown in Figure 11. The analysis of the position of the magnetic reflections indicated that the corresponding magnetic structure is defined by the propagation vector $\boldsymbol{k}$ = (½ 0 0). The propagation vector was calculated by using K_SEARCH and the irreducible representations, suitable with the space-group $P\bar{3}m1$ and the propagation vector, and the associated basis vectors were generated using the program BasIreps. The magnetic ions hosted by this compound are preferentially ordered forming Ru_2O_9 dimers with the Ru cations occupying the 2*d* (1/3, 2/3, z) Wyckoff position, however there is a certain percentage of Ru located at the 1*a* (0,0,0) site. As shown in Table 4, the magnetic symmetry on ruthenium sites decomposes as (in BasIReps numbering): $\Gamma^1+\Gamma^2+\Gamma^3+\Gamma^4$ for Ru (1/3, 2/3, z) and $\Gamma^1+\Gamma^3$ for Ru (0,0,0). Among all the possible combinations, the spin structure that fits best the main magnetic reflections (00l) corresponds to Γ^3 (Ψ_2) basis, where the Ru spins are laying on the *ab*-plane. The obtained magnetic moment components along the *a*- and *b*-axis are m_x = 1.3(1) μ_B and m_y = 0.65(8) μ_B for Ru at the dimer positions and m_x = 0.7(2) and m_y = 0.3(1) μ_B for Ru(000) and the resultant moment of 1.5(1) μ_B and 0.8(2) μ_B respectively. As is the case for Ba_2FeOsO_6 [40] there is no evidence that the spins at the two sites align at different temperatures. That the spins are aligned in the a*b*-plane is significantly different to that seen in Ba_2FeOsO_6 where the spins align along the *c*-axis, although the reason for this is unclear. The value of the magnetic moment estimated from the Curie-Weiss fitting of the susceptibility data between 200 and 300 K is 3.1 μB and θ_c = -235 K. which gives a remarkably high frustration index of 29.

Table 4. Irreducible representations and basis vectors of the hexagonal $P\bar{3}m1$ space group associated to the propagation vector $\boldsymbol{k}$ = (½ 0 0) for the Ru atoms at the 2*d* and 1*a* sites.

		Ru1(x,y,z)$_{2d}$			Ru2(-x, -y, z+1/2)$_{2d}$			Ru3(0, 0, 0)$_{1a}$		
Irreducible representation	Basis vectors	m_x	m_y	m_z	m_x	m_y	m_z	m_x	m_y	m_z
Γ^1	Ψ_1	0	-1	0	0	-1	0	0	-1	0
Γ^2	Ψ_1	2	1	0	-2	-1	0			
	Ψ_2	0	0	1	0	0	-1		-	
Γ^3	Ψ_1	2	1	0	2	1	0	2	1	0
	Ψ_2	0	0	1	0	0	1	0	0	1
Γ^4	Ψ_1	0	-1	0	0	1	0		-	

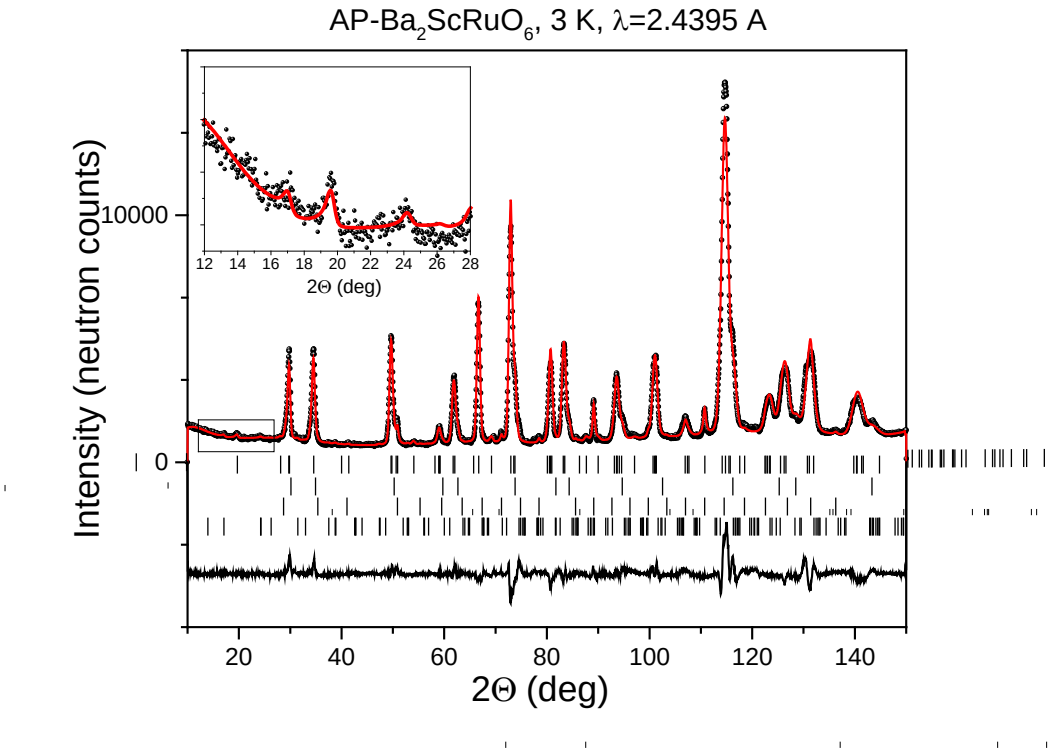

Figure 11. Observed (symbols), calculated (red line), and difference (black line) NPD Rietveld profiles for AP-Ba_2ScRuO_6 at 3 K. The upper series of Bragg reflections corresponds to the main hexagonal perovskite phase, the second to the cubic structure, the third to the Sc_2O_3 impurity and the lower to the magnetic structure.

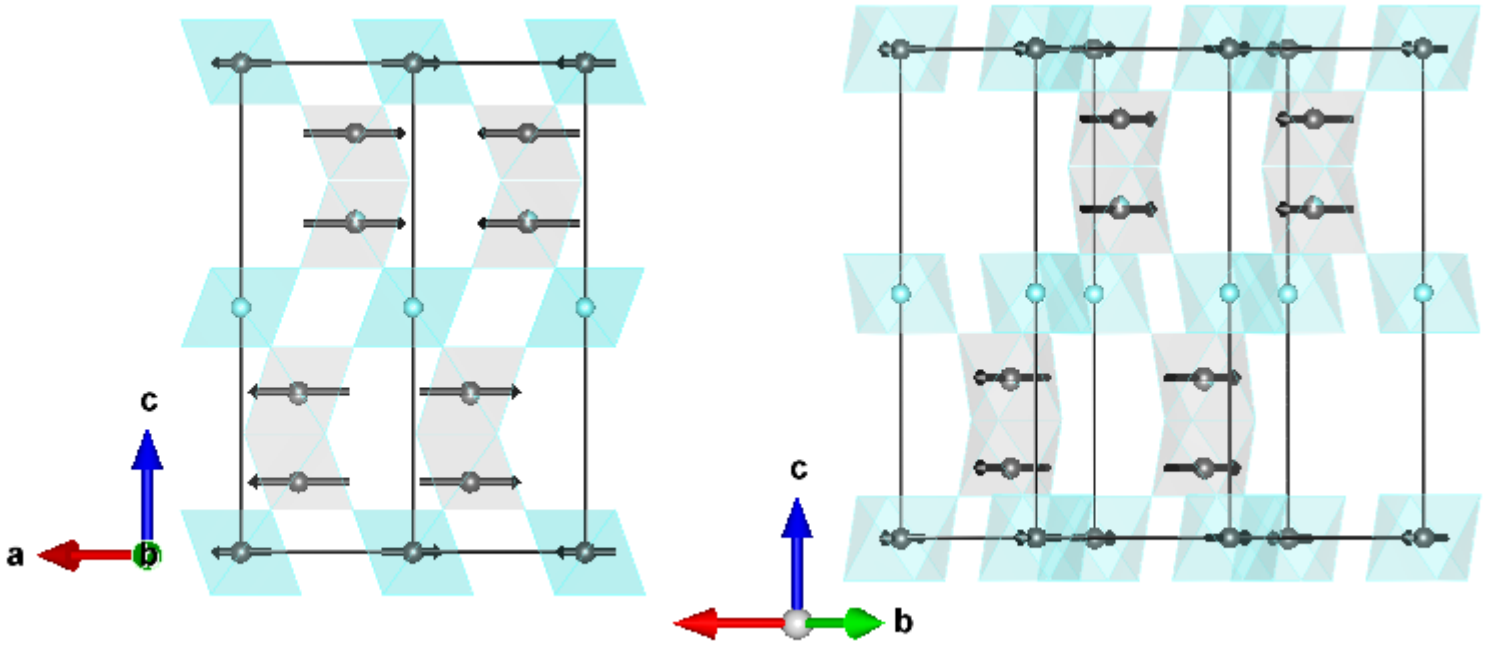

Figure 12. Schematic view of the magnetic structure of AP-Ba_2ScRuO_6 below T_N.

Discussion and Concluding Remarks

The refined values of the magnetic moment for HP-Ba_2ScRuO_6 (2.04(5) μ_B) and Sr_2ScRuO_6 (1.97(2) μ_B) are comparable to those reported for similar Ru^{5+} double perovskites of 2μ_B [11], 2.1(1) [47] and 2.05(4) μ_B [15] and is significantly reduced from the expected spin-only value of 3μ_B. This reduction in the magnetic moment is mainly a consequence of covalency effects between the Ru 4*d* and O 2p orbitals. However, the possibility that this is strongly impacted by the effects of spin-orbit coupling, which are believed to play an important role in $4d^3$ transition metals as reported by Carlo *et al.* [19] should not be discounted. For the AP-Ba_2ScRuO_6 polymorph, the magnetic moment, 1.5(1) μ_B and 0.8(2) μ_B corresponding to Ru placed at the shared-corner and the shared-face octahedral respectively, is considerable lower than the theoretical moment and it is similar to the one obtained for the other hexagonal perovskites containing Ru_2O_9 dimers, such as $Ba_3LaRu_2O_9$ and $Ba_3YRu_2O_9$ compounds [38], 1.4(2) μ_B and 0.5(6) μ_B respectively, and it is ascribed to certain degree of spin frustration.

Considering the present results in the light of those already available, a number of observations regarding the influence of non-magnetic cations on the magnetism in 4*d* and 5*d* oxides can be made. That Sr_2ScRuO_6 adopts a corner-sharing perovskite motif and Ba_2ScRuO_6 a face-sharing hexagonal motif when prepared at ambient pressure reflects the differences in the familiar perovskite tolerance factor, *t* (0.966 vs 1.024 respectively). Only when $t \sim 1$ is the ideal un-tilted perovskite structure observed, values of $t < 1$ indicate the structure is likely to be stabilized by cooperative tilting of the corner sharing octahedra and if $t > 1$ hexagonal packing (face sharing) is favored. The use of high-pressure-temperature conditions during synthesis favors corner sharing and this has been used previously to promote a corner sharing perovskite motif over a face sharing (hexagonal) motif, including the preparation of a trigonal corner sharing polymorph of $Ba_3NaRu_2O_9$ and $Sr_3CaRu_2O_9$ rather than the 6H-hexagonal structure favored by ambient pressure synthesis [48 49]. A similar situation is observed here. That the analogous Ir oxides (Sr_2ScIrO_6 t = 0.962 SG $P2_1/n$ and Ba_2ScIrO_6 t = 1.020 $Fm\bar{3}m$) prepared at ambient pressure have different structures reflects the flexibility of the perovskite structure. Whilst Ba_2ScOsO_6 (t = 1.026) does not seem to have been prepared it is reasonable to speculate that this too will adopt a hexagonal type structure if prepared at ambient pressure. Likewise Sr_2ScOsO_6 t = 0.968 that is reported to be monoclinic in $P2_1/n$ at room temperature is likely to

transform to the *I*2/*m* monoclinic structure, observed for Sr_2ScRuO_6, if heated to above room temperature.

Neel temperatures and ordered magnetic moments for the family of oxides $A_2BB'O_6$ *A* = Ba or Sr, *B* = Y or Sc and *B*' = Ru or Os are collected in Table 5. All of these oxides exhibit a type-I antiferromagnetic structure. From Table 5 it is apparent that a higher Neel temperature is observed for Sc rather than Y containing oxides, for Os than Ru and for Sr than Ba, although the pair Sr_2YRuO_6/Ba_2YRuO_6 violates the last relationship. In the first case, this tendency can be explained in terms of the d^n electron occupancy of the non-magnetic *B* metal. Its electronic configuration is directly related to the hybridization of the *B*/*B*' cation states, being stronger for open shell d^0 metals. The larger hybridization enhances the *B* and *B*' orbital overlapping and thus improves the exchange interactions. In the second case, the higher T_N for the Os compounds is also associated with hybridization effects, which is higher in 5*d* metals rather than in 4*d*, and in the third one, this observation may be due to the balance between the geometrically frustrated *B* sublattice, more noticeable in cubic symmetries, and the deviation of the super exchange angle to the ideal value of 180 degrees. The larger reduction in ordered moments from the spin only value in the Os oxides than in the Ru oxides is a result of both the increased covalence or hybridization of the M-O bond in Os due to the more diffuse nature of the 5*d* orbitals and the greater SOC constant for Os^{5+} [50, 51].

Table 5. Neel temperatures and ordered magnetic moments derived from neutron diffraction for some rock-salt ordered $A_2BB'O_6$ double perovskites.

Oxide	T_N (K)	Ordered Moment	Reference
Sr_2ScRuO_6	60	1.97(2)	This work
Sr_2YRuO_6	26	1.96	[44]
Sr_2ScOsO_6	92	1.6(1)	[26]
Sr_2YOsO_6	53	1.91(3)	[26]
Ba_2ScRuO_6	43	2.04(5)	This work
Ba_2YRuO_6	36	2.2(1)	[11]
Ba_2YOsO_6	36	1.65(5)	[50]
Ba_2ScOsO_6	93	-	[51]

The effective ionic radii of Os^{5+} and Ru^{5+} are expected to be similar as a consequence of the lanthanoid contraction. This expectation is validated by comparing the volume of suitably matched pairs. Consequently the structures are very similar, nevertheless the Neel temperatures for the osmates

are systematically higher. Inelastic Neutron Scattering of Sr_2ScOsO_6 suggests that a combination of Near Neighbor antiferromagnetic interactions together with SOC and strong *M*-O hybridization are responsible [25]. DFT calculations [27] suggest that the exchange coupling is strongly dependent on the overlap between the Os-5*d* and Sc/Y 3*d*/4*d* states where the hybridization of the Sc 3*d* states with the Os 5*d* states is greater than that for the Y 4*d* states. The present results suggest the same is true for overlap between the Ru 4*d* and Sc/Y 3*d*/4*d* states.

Acknowledgments

This research was supported in part by the Australian Research Council, the World Premier International Research Center Initiative (WPI Initiative, MEXT, Japan) and the Japan Society for the Promotion of Science (JSPS) through the Grants in-Aid for Scientific Research (15K14133, 16H04501). The work was, in part, performed at the Powder Diffraction beamline at the Australian Synchrotron. We thank Drs Quifen Gu and Justin Kimpton for their assistance with these measurements.

References

(1) Longo, J. M.; Raccah, P. M.; Goodenough, J. B. Magnetic Properties Of $SrRuO_3$ And $CaRuO_3$. *J. Appl. Phys.* , **1968,** 39, 1327.

(2) Dabrowski, B.; Kolesnik, S.; Chmaissem, O.; Maxwell, T.; Avdeev, M.; Barnes, P. W.; Jorgensen, J. D. Increase of ferromagnetic ordering temperature by the minority-band double-exchange interaction in $SrRu_{1-x}Cr_xO_3$. *Phys. Rev. B:,* **2005,** 72, 054428.

(3) Pi, L.; Maignan, A.; Retoux, R.; Raveau, B. Substitution at the Ru site in the itinerant ferromagnet $SrRuO_3$. *J. Phys.: Condens. Matter* **2002,** 14, 7391-7398.

(4) Seki, H.; Yamada, R.; Saito, T.; Kennedy, B. J.; Shimakawa, Y. High-Concentration Na Doping of $SrRuO_3$ and $CaRuO_3$. *Inorg. Chem.,* **2014,** 53, 4579-4584.

(5) Vasala, S.; Karppinen, M. $A_2B'B''O_6$ perovskites: A review. *Prog. Solid State Chem.,* **2015,** 43, 1-36.

(6) Anderson, M. T.; Greenwood, K. B.; Taylor, G. A.; Poeppelmeier, K. R. B-cation arrangements in double perovskites. *Prog. Solid State Chem.,* **1993,** 22, 197-233.

(7) Dass, R. I.; Yan, J. Q.; Goodenough, J. B. Ruthenium double perovskites: Transport and magnetic properties. *Phys. Rev. B:,* **2004,** 69, 094416.

(8) Hinatsu, Y.; Izumiyama, Y.; Doi, Y.; Alemi, A.; Wakeshima, M.; Nakamura, A.; Morii, Y. Studies on magnetic and calorimetric properties of double perovskites Ba_2HoRuO_6 and Ba_2HoIrO_6. *J. Solid State Chem.,* **2004,** 177, 38-44.

(9) Hong, K. P.; Choi, Y. H.; Kwon, Y. U.; Jung, D. Y.; Lee, J. S.; Shim, H. S.; Lee, C. H. Atomic and magnetic long-range orderings in $BaLaMRuO_6$ (M = Mg and Zn). *J. Solid State Chem.,* **2000,** 150, 383-390.

(10) Battle, P. D.; Goodenough, J. B.; Price, R. The Crystal-Structures And Magnetic-Properties Of Ba_2LaRuO_6 And Ca_2LaRuO_6. *J. Solid State Chem.,* **1983,** 46, 234-244.

(11) Battle, P. D.; Jones, C. W. The Crystal And Magnetic-Structures Of Sr_2LuRuO_6, Ba_2YRuO_6, And Ba_2LuRuO_6. *J. Solid State Chem.,* **1989,** 78, 108-116.

(12) Battle, P. D.; Macklin, W. J. The Crystal And Magnetic-Structures Of Sr_2YRuO_6. *J. Solid State Chem.,* **1984,** 52, 138-145.

(13) Disseler, S. M.; Lynn, J. W.; Jardim, R. F.; Torikachvili, M. S.; Granado, E. Spin dynamics and two-dimensional correlations in the fcc antiferromagnetic Sr_2YRuO_6. *Phys. Rev. B:* , **2016,** 93, 140407.

(14) Aczel, A. A.; Baker, P. J.; Bugaris, D. E.; Yeon, J.; Loye, H. C. Z.; Guidi, T.; Adroja, D. T. Exotic Magnetism on the Quasi-fcc Lattices of the d^3 Double Perovskites $La_2NaB'O_6$ (B' = Ru, Os). *Phys. Rev. Lett.* , **2014,** 112, 117603.

(15) Nilsen, G. J.; Thompson, C. M.; Ehlers, G.; Marjerrison, C. A.; Greedan, J. E. Diffuse magnetic neutron scattering in the highly frustrated double perovskite Ba_2YRuO_6. *Phys. Rev. B:,* **2015,** 91, 054415.

(16) Ranjbar, B.; Pavan, A.; Kennedy, B. J.; Zhang, Z. M. Structural and magnetic properties of the ruthenium double perovskites $Ba_{2-x}Sr_xYRuO_6$. *Dalton Trans.* , **2015,** 44, 10689-10699.

(17) Granado, E.; Lynn, J. W.; Jardim, R. F.; Torikachvili, M. S. Two-Dimensional Magnetic Correlations and Partial Long-Range Order in Geometrically Frustrated Sr_2YRuO_6. *Phys. Rev. Lett.* , **2013,** 110, 017202.

(18) Takahashi, R.; Okazaki, R.; Yasui, Y.; Terasaki, I.; Sudayama, T.; Nakao, H.; Yamasaki, Y.; Okamoto, J.; Murakami, Y.; Kitajima, Y. High-temperature thermoelectric properties of the double-perovskite ruthenium oxide $(Sr_{1-x}La_x)_2ErRuO_6$. *J. Appl. Phys.* , **2012,** 112, 073714.

(19) Carlo, J. P.; Clancy, J. P.; Fritsch, K.; Marjerrison, C. A.; Granroth, G. E.; Greedan, J. E.; Dabkowska, H. A.; Gaulin, B. D. Spin gap and the nature of the $4d^3$ magnetic ground state in the frustrated fcc antiferromagnet Ba_2YRuO_6. *Phys. Rev. B:,* **2013,** 88, 024418.
(20) Gemmill, W. R.; Smith, M. D.; Prozorov, R.; Loye, H. C. Z. Crystal growth and magnetic properties of lanthanide-containing osmium double perovskites, Ln_2NaOsO_6 (Ln = La, Pr, Nd). *Inorg. Chem.,* **2005,** 44, 2639-2646.
(21) Kayser, P.; Martinez-Lope, M. J.; Alonso, J. A.; Retuerto, M.; Croft, M.; Ignatov, A.; Fernandez-Diaz, M. T. Crystal Structure, Phase Transitions, and Magnetic Properties of Iridium Perovskites $S_{r2}MIrO_6$ (M = Ni, Zn). *Inorg. Chem.*, **2013,** 52, 11013-11022.
(22) Matsuura, H.; Miyake, K. Effect of Spin–Orbit Interaction on $4d^3$- and $5d^3$ Based Transition-Metal Oxides. *J. Phys. Soc. Jpn. ,* **2013,** 82, 073703.
(23) Thompson, C. M.; Marjerrison, C. A.; Sharma, A. Z.; Wiebe, C. R.; Maharaj, D. D.; Sala, G.; Flacau, R.; Hallas, A. M.; Cai, Y.; Gaulin, B. D.; Luke, G. M.; Greedan, J. E. Frustrated magnetism in the double perovskite La_2LiOsO_6: A comparison with La_2LiRuO_6. *Phys. Rev. B:,* **2016,** 93, 014431.
(24) Taylor, A. E.; Morrow, R.; Fishman, R. S.; Calder, S.; Kolesnikov, A. I.; Lumsden, M. D.; Woodward, P. M.; Christianson, A. D. Spin-orbit coupling controlled ground state in Sr_2ScOsO_6. *Phys. Rev. B:,* **2016,** 93, 220408.
(25) Taylor, A. E.; Morrow, R.; Singh, D. J.; Calder, S.; Lumsden, M. D.; Woodward, P. M.; Christianson, A. D. Magnetic order and electronic structure of the $5d^3$ double perovskite Sr_2ScOsO_6. *Phys. Rev. B:,* **2015,** 91, 100406.
(26) Paul, A. K.; Sarapulova, A.; Adler, P.; Reehuis, M.; Kanungo, S.; Mikhailova, D.; Schnelle, W.; Hu, Z. W.; Kuo, C. Y.; Siruguri, V.; Rayaprol, S.; Soo, Y. L.; Yan, B. H.; Felser, C.; Tjeng, L. H.; Jansen, M. Magnetically Frustrated Double Perovskites: Synthesis, Structural Properties, and Magnetic Order of Sr_2BOsO_6 (B = Y, In, Sc). *Z. Anorg. Allg. Chem. ,* **2015,** 641, 197-205.
(27) Kanungo, S.; Yan, B. H.; Felser, C.; Jansen, M. Active role of nonmagnetic cations in magnetic interactions for double-perovskite Sr_2BOsO_6 (B = Y, In, Sc). *Phys. Rev. B:,* **2016,** 93, 161116.
(28) Wallwork, K. S.; Kennedy, B. J.; Wang, D. The high resolution powder diffraction beamline for the Australian Synchrotron. *AIP Conf. Proceed.,* **2007,** 879, 879-882.
(29) Liss, K.-D.; Hunter, B.; Hagen, M.; Noakes, T.; Kennedy, S. Echidna - the new high-resolution powder diffractometer being built at OPAL. *Physica B,* **2006,** 385-86, 1010-1012.
(30) Larson, A. C.; Von Dreele, R. B. GSAS. **1994**.
(31) Toby, B. H. EXPGUI, a graphical user interface for GSAS. *J. Appl. Crystallogr.,* **2001,** 34, 210-213.
(32) Rodriguez-Carvajal, J. Recent Advances In Magnetic-Structure Determination By Neutron Powder Diffraction. *Physica B,* **1993,** 192, 55-69.
(33) Parkinson, N. G.; Hatton, P. D.; Howard, J. A. K.; Ritter, C.; Chien, F. Z.; Wu, M. K. Crystal and magnetic structures of $A_2YRu_{1-x}Cu_xO_6$ with A = Sr, Ba and x = 0.05 to 0.15. *J. Mater. Chem.,* **2003,** 13, 1468-1474.
(34) Howard, C. J.; Kennedy, B. J.; Woodward, P. M. Ordered double perovskites - a group-theoretical analysis. *Acta Crystallogr., Sect. B: Struct. Sci* **2003,** 59, 463-471.
(35) Kayser, P.; Ranjbar, B.; Kennedy, B. J.; Kimpton, J. A.; Avdeev, M. Spin-orbit coupling controlled ground state in the Ir^V perovskites A_2ScIrO_6 (A = Ba or Sr) *Inorg. Chem.,* **2017,** 56, 2204-2209.
(36) Bader, H.; Kemmler-Sack, S. Über Sauerstoffperowskite des fünfwertigen Rutheniums $A_2B^{III}Ru^VO_6$ mit A = Ba, Sr. *Z. Anorg. Allg. Chem. ,* **1980,** 466, 97-102.

(37) Hinatsu, Y.; Doi, Y. Structures and Magnetic Properties of Double Perovskites A_2LnMO_6 and 6H-Perovskites $Ba_3LnRu_2O_9$ (A = Sr, Ba; Ln = Y, Lanthanides; M = Nb, Ta, Ru). *Bull. Chem. Soc. Jpn.,* **2003,** 76, 1093-1113.
(38) Senn, M. S.; Kimber, S. A. J.; Lopez, A. M. A.; Hill, A. H.; Attfield, J. P. Spin orders and lattice distortions of geometrically frustrated 6H-perovskites $Ba_3B'Ru_2O_9$ (B' = La^{3+}, Nd^{3+}, and Y^{3+}). *Phys. Rev. B:,* **2013,** 87, 134402.
(39) Miiller, W.; Avdeev, M.; Zhou, Q. D.; Studer, A. J.; Kennedy, B. J.; Kearley, G. J.; Ling, C. D. Spin-gap opening accompanied by a strong magnetoelastic response in the S=1 magnetic dimer system $Ba_3BiRu_2O_9$. *Phys. Rev. B:,* **2011,** 84, 220406.
(40) Feng, H. L.; Adler, P.; Reehuis, M.; Schnelle, W.; Pattison, P.; Hoser, A.; Felser, C.; Jansen, M. High-Temperature Ferrimagnetism with Large Coercivity and Exchange Bias in the Partially Ordered 3d/5d Hexagonal Perovskite $Ba_2Fe_{1.12}Os_{0.88}O_6$. *Chem. Mater.,* **2017,** 29, 886-895.
(41) Ivanov, S. A.; Nordblad, P.; Mathieu, R.; Tellgren, R.; Ritter, C. Neutron diffraction studies and the magnetism of an ordered perovskite: Ba_2CoTeO_6. *Dalton Trans. ,* **2010,** 39, 5490-5499.
(42) Kayser, P.; Injac, S.; Kennedy, B. J.; Menezes de Oliveira, A. L.; Shirako, Y.; Hasegawa, M. Thermal expansion in $BaRuO_3$ perovskites - an unusual case of bond strengthening at high temperatures. *Dalton Trans. ,* **2017,** 46, 2974-2980.
(43) Santoro, A.; Natali Sora, I.; Huang, Q. Bond valence analysis of $BaRuO_3$. *J. Solid State Chem.,* **2000,** 151, 245-252.
(44) Stitzer, K. E.; El Abed, A.; Smith, M. D.; Davis, M. J.; Kim, S. J.; Darriet, J.; zur Loye, H. C. Crystal growth of novel osmium-containing triple perovskites. *Inorg. Chem,,* **2003,** 42, 947-949.
(45) Mogare, K. M.; Klein, W.; Jansen, M. $K_2NaOsO_{5.5}$ and $K_3NaOs_2O_9$: The first osmium perovskites containing alkali cations at the "A" site. *J. Solid State Chem.,* **2012,** 191, 153-157.
(46) Kayser, P.; Ranjbar, B.; Kennedy, B. J.; Avdeev, M. The impact of chemical doping on the magnetic state of the Sr_2YRuO_6 double perovskite *J. Solid State Chem.,* **2017,** 249, 154-159.
(47) Aharen, T.; Greedan, J. E.; Ning, F.; Imai, T.; Michaelis, V.; Kroeker, S.; Zhou, H. D.; Wiebe, C. R.; Cranswick, L. M. D. Magnetic properties of the S=3/2 geometrically frustrated double perovskites La_2LiRuO_6 and Ba_2YRuO_6. *Phys. Rev. B:,* **2009,** 80, 134423.
(48) Arevalo-Lopez, A. M.; Senn, M. S.; Skedd, L.; Attfield, J. P. High Pressure Synthesis of the Cation-ordered Perovskite 3C1:2-$Ba_3NaRu_2O_9$. *Z. Anorg. Allg. Chem. ,* **2014,** 640, 1164-1167.
(49) Rijssenbeek, J. T.; Saito, T.; Malo, S.; Azuma, M.; Takano, M.; Poeppelmeier, K. R. Effect of Explicit Cationic Size and Valence Constraints on the Phase Stability of 1:2 B-Site-Ordered Perovskite Ruthenates. *J. Am. Chem. Soc. ,* **2005,** 127, 675-681.
(50) Kermarrec, E.; Marjerrison, C. A.; Thompson, C. M.; Maharaj, D. D.; Levin, K.; Kroeker, S.; Granroth, G. E.; Flacau, R.; Yamani, Z.; Greedan, J. E.; Gaulin, B. D. Frustrated fcc antiferromagnet Ba_2YOsO_6: Structural characterization, magnetic properties, and neutron scattering. *Phys. Rev. B:,* **2015,** 91, 075133.
(51) Feng, H. L.; Yamaura, K.; Tjeng, L. H.; Jansen, M. The role of nonmagnetic d^0 vs. d^{10} B-type cations on the magnetic exchange interactions in osmium double perovskites. *J. Solid State Chem.,* **2016,** 243, 119-123.

-For Table of Contents Only-

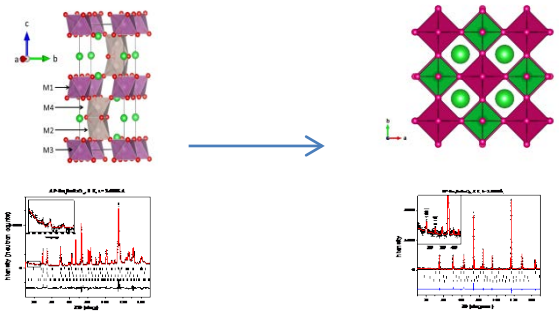

The synthesis, structural and magnetic properties of some ruthenium containing double perovskites A_2ScRuO_6 are described. The ambient pressure hexagonal and high pressure cubic polymorphs of Ba_2ScRuO_6 exhibit different magnetic and electronic properties, cubic Ba_2ScRuO_6 displays a metal-insulator transition near 270 K and hexagonal Ba_2ScRuO_6 is a semiconductor. Sr_2ScRuO_6 is non-metallic. All three oxides are antiferromagnets. Hexagonal Ba_2ScRuO_6 has partial Sc-Ru ordering at both the face-sharing B_2O_9 dimer and corner sharing BO_6 sites.